Infrared Spectrum of Nitric Acid Dihydrate: Influence of Particle Shape

Robert Wagner,* Ottmar Möhler, Harald Saathoff, Olaf Stetzer, and Ulrich Schurath

Forschungszentrum Karlsruhe, Institute of Meteorology and Climate Research (IMK-AAF), Karlsruhe, Germany

Received: November 2, 2004; In Final Form: January 17, 2005

In situ Fourier transform infrared (FTIR) extinction spectra of airborne α-NAD microparticles generated by two different methods were recorded in the large coolable aerosol chamber AIDA of Forschungszentrum Karlsruhe. The extinction spectrum of α-NAD crystals obtained by shock freezing of a HNO_3/H_2O gas mixture could be accurately reproduced using Mie theory with published refractive indices of α-NAD as input. In contrast, Mie theory proved to be inadequate to properly reproduce the infrared extinction spectrum of α-NAD crystals which were formed via homogeneous nucleation of supercooled HNO_3/H_2O solution droplets, evaporating slowly on a time scale of several hours at about 195 K. Much better agreement between measured and calculated extinction spectra was obtained by T-matrix calculations assuming oblate particles with aspect ratios greater than five. This indicates that strongly aspherical α-NAD crystals are obtained when supercooled nitric acid solution droplets freeze and grow slowly, a process which has been discussed as a potential pathway to the formation of crystalline polar stratospheric cloud (PSC) particles.

Introduction

Satellite observations in the mid-infrared may improve our knowledge about the composition, phase, volume, and size distribution of polar stratospheric cloud (PSC) constituents.[1] At temperatures above the ice frost point, PSC particles are believed to be composed of either supercooled ternary $H_2SO_4/H_2O/HNO_3$ solution droplets (type Ib) or crystals of nitric acid tri- or dihydrate (NAT or NAD, type Ia).[2−4] The retrieval of PSC particle microphysical properties from the measured infrared spectra relies on accurate reference spectra of the various components, based on optical constants which have been determined in the laboratory. These refractive index data are usually inferred from either thin-film measurements[5,6] or actual aerosol infrared spectra.[7−9] Often, retrieval algorithms apply Mie theory to analyze aerosol extinction spectra in the mid-infrared,[1,10] although PSC type Ia particles are characterized by strong depolarization in lidar observations, clearly indicating aspherical particle shapes.[2,11−13] Richwine et al.[9] and Niedziela et al.[7] conclude in their studies about the infrared spectra of NAT and NAD that by averaging over a particle size distribution the sensitivity to particle shape may be removed. In the present contribution, however, we will show on the basis of measured infrared spectra of laboratory-generated NAD particles that depending on the formation conditions the application of Mie theory may not be adequate to accurately reproduce our recorded spectra.

When interpreting variations in the infrared spectra of nitric acid dihydrate particles, two different NAD modifications have to be taken into account. Only recently, it has been established that nitric acid dihydrate crystallizes in a low- and high-temperature phase, showing similar layer structures but differing in the H bond structure between neighboring layers.[14,15] Tizek et al.[16] carefully investigated the crystallization behavior of these so-called α- and β-NAD phases by X-ray powder diffraction, thereby preparing the ground for their recent spectroscopic study dealing with differences in the infrared spectra of the two NAD modifications.[17] In their study, HNO_3/H_2O aerosol particles were shock frozen on a cold sample support at 80 K. Subsequent annealing to >180 K led to the crystallization of the two NAD phases with a phase distribution which was crucially influenced by the initial composition of the quenched solution droplets. When starting with a 1:2 HNO_3:H_2O molar ratio, almost pure β-NAD was formed upon annealing to 180 K. In contrast, nonstoichiometric compositions favored the crystallization of α-NAD, which, however, was never produced as a pure phase. The new spectroscopic results of Tizek et al.[16] may primarily account for the notable dependence of the NAD infrared spectra on formation conditions and temperature, as shown in the spectra collection by Tisdale et al.[18] (see Figure 4 therein). The published optical constants of NAD from the studies of Toon et al.[5] (retrieved from IR spectra of crystalline thin films at 184 K) and Niedziela et al.[7] (obtained from particle spectra in a laminar flow cell at $T = 190-160$ K) both clearly reveal the spectroscopic signatures characteristic of the α-NAD modification: (i) the ν_1 nitrate vibration at about 1030 cm^{-1}, which is significantly shifted to 1040 cm^{-1} in β-NAD; (ii) the doublet feature at around 3490 and 3260 cm^{-1} in the OH stretching regime,[19,20] where β-NAD shows three bands at 3490, 3392, and 3175 cm^{-1}; (iii) the asymmetric deformation mode of the H_3O^+ ion at 1740 cm^{-1}, located at 1850 cm^{-1} in the spectrum of β-NAD; and (iv) the position of the low-frequency component of the characteristic ν_3 nitrate doublet at about 1270 cm^{-1}, which is clearly shifted to higher wavenumbers (about 1340 cm^{-1}) for β-NAD. Infrared spectra of annealed films or particles in the Tisdale et al.[18] spectra collection bare some characteristics of β-NAD, indicating a phase transition into the high temperature β-NAD modification.

In addition to the different spectral signatures of α- and β-NAD, we want to emphasize the effect of particle shape on band positions and intensities in infrared spectra of NAD. In our present study, as part of ongoing laboratory measurements of PSC particles in the large coolable aerosol chamber AIDA of Forschungszentrum Karlsruhe,[21−24] we have generated α-NAD

* To whom correspondence should be addressed. E-mail: Robert.Wagner@imk.fzk.de.

10.1021/jp044997u CCC: $30.25
Published on Web 02/23/2005

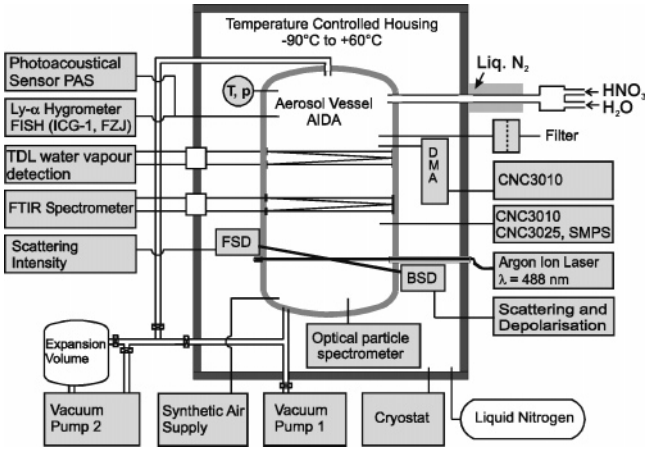

Figure 1. Schematic view of the AIDA aerosol chamber facility, showing the major instrumentation used in the PSC experiments, as described in detail by Möhler et al.[21,25] The cylindrical aluminum vessel, volume 84 m^3, is mounted inside a large isolating housing, whose temperature can be adjusted between 330 and 183 K. For the present experiments, a gaseous mixture of HNO_3/H_2O in synthetic air was injected into the chamber. In experiments B1 and B2, the gas injection tube was at room temperature, whereas in experiment A, it was cooled with liquid nitrogen.

particles in two different ways: (1) by shock freezing a HNO_3/H_2O gas mixture and (2) by homogeneous nucleation of slowly evaporating supercooled HNO_3/H_2O solution droplets at constant temperature on a time scale of several hours. The recorded FTIR extinction spectra of the NAD particles were analyzed by Mie theory as well as T-matrix calculations assuming spheroidal particle shapes with the aspect ratio as adjustable parameter. We will show that depending on the formation conditions of the NAD crystals our measured infrared spectra could only be accurately reproduced assuming strongly aspherical particle shapes. Implications of our findings for atmospheric applications will be discussed.

Methods

Experimental. The presented experiments were performed in the low-temperature aerosol chamber facility AIDA (Aerosol Interactions and Dynamics in the Atmosphere) of Forschungszentrum Karlsruhe, which can be cooled to a minimum temperature of about 183 K to simulate conditions prevailing in the polar winter stratosphere. The instrumentation of the chamber for our PSC simulation experiments is shown in Figure 1. The large volume of 84 m^3 permitted experiments on time scales of several hours, much longer than previously reported laboratory studies of airborne nitric acid hydrate particles. In the present study, we will focus on results of FTIR extinction measurements; for a detailed description of the entire AIDA technical equipment, the reader is referred to recent publications.[21,25] Using a White-type multiple reflection cell, mounted at medium height in the aerosol vessel, infrared extinction spectra of the investigated aerosol particles were measured in situ using a horizontal optical path length of about 250 m. This yielded infrared spectra with good signal-to-noise ratios at low particle densities of typically 100−10 000 cm^{-3}. Spectra were recorded with a FTIR spectrometer (Bruker, IFS 66v) in the 6000−800 wavenumber range with a resolution of 4 cm^{-1}.

As already indicated in the introductory section, NAD particles were generated by two different methods. In both cases, two synthetic air flows of 1 L/min were passed over thermostated reservoirs of nitric acid and water. In experiment A, the combined carrier gases were injected into the AIDA chamber

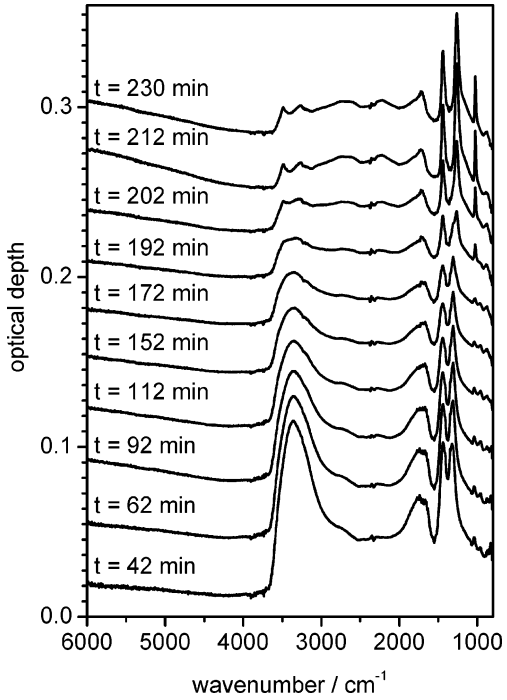

Figure 2. Series of FTIR spectra documenting the slow conversion of a supercooled HNO_3/H_2O solution droplet aerosol to α-NAD at $T = 195$ K (later on referred to as experiment B2). Individual spectra are offset for clarity. Denoted are the times after the start of aerosol inlet. The initial composition of the nitric acid droplets was about 45 wt % HNO_3, as derived from Mie fits using the optical constants from Norman et al.[26] Due to the higher wall loss rate of H_2O(g) compared to HNO_3(g), the nitric acid mass fraction continuously increased up to about 57 wt % at $t = 172$ min. α-NAD spectral signatures can be clearly observed for the first time at $t = 192$ min.

after passing through a liquid-nitrogen-cooled tube section. The chamber was held at a temperature of 195 K (Figure 1). This approach resulted in small particles formed by binary homogeneous nucleation of the supersaturated nitric acid/water vapor mixture. As previously reported by Niedziela et al.,[7] we were able to generate pure NAD particles when choosing a molar ratio H_2O:HNO_3 of about three in the combined carrier gases. The FTIR spectrum of this NAD aerosol will be presented in the next section where the spectroscopic signatures of NAD particles obtained by different formation techniques are compared (Figure 3). The spectrum obtained in experiment A has been chosen as a reference, demonstrating the suitability of the AIDA instrumentation to study the formation of NAD aerosol particles on the basis of their FTIR spectra, thereby preparing the ground for experiments of type B.

Type B experiments were designed to determine homogeneous nucleation rates of supercooled HNO_3/H_2O solution droplets. The droplet aerosol was prepared by directly injecting the warm gaseous nitric acid/water mixture into the particle-free (<0.1 particles cm^{-3}) cold ($T < 200$ K) and dry chamber air for typically about 15 min. Nitric acid droplets directly formed by nucleation and condensation of the supersaturated HNO_3 and water vapors. Several experiments were performed at different chamber temperatures, covering a range of $T = 190$−198 K. In each study, the temporal evolution of aerosol composition and phase was monitored by continuous FTIR extinction measurements.

Figure 2 shows a time sequence of infrared spectra for an experiment conducted at $T = 195$ K. During the first ca. 150 min, the droplet aerosol became more concentrated in HNO_3 by slowly loosing water vapor to the chamber walls. Qualita-

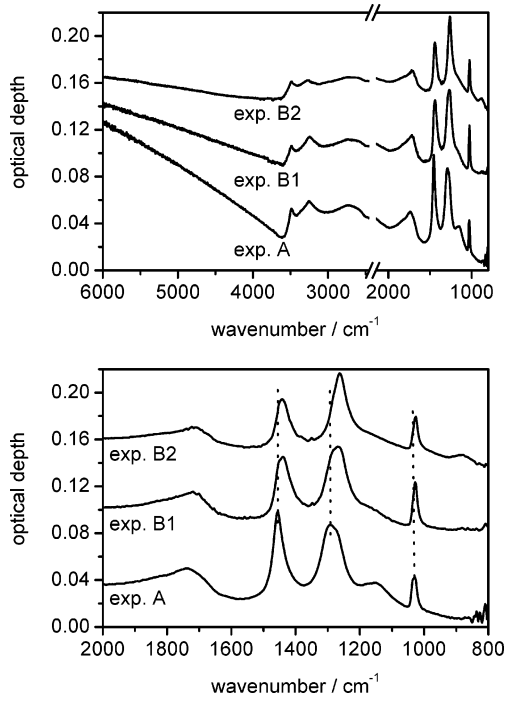

Figure 3. Different infrared spectra of airborne NAD crystals generated in the present study. The CO_2(g) absorption regime is omitted. The lower panel shows an expanded view from 2000 to 800 cm^{-1}. In experiment A, NAD particles were generated by shock freezing of the vapors at liquid nitrogen temperature. The slow homogeneous nucleation of NAD from supercooled HNO_3/H_2O solution droplets at $T = 193$ and 195 K was studied in experiments B1 and B2.

tively, this is evidenced by the increasing intensity of the characteristic doublet extinction feature of the nitrate ion between 1300 and 1500 cm^{-1} in relation to the OH stretching regime at about 3300 cm^{-1}. After about 3 h, further notable changes occurred in the spectral signatures, indicating that a significant fraction of the supercooled HNO_3/H_2O droplets had frozen to become detectable in the infrared spectra. Here, the sharp 1030 cm^{-1} ν_1 nitrate vibration serves as a sensitive marker for the freezing of the solution droplets to α-NAD. About 30 min later, the FTIR spectra indicated complete freezing of the nitric acid droplets, as confirmed by additional size distribution measurements with an optical particle counter, documenting that the initial cloud of sub-μm supercooled liquid droplets (count median diameter ~0.2 μm) had been replaced by a new particle mode with optical diameters between 1 and 10 μm. Thereafter, no further changes in the infrared spectra of the NAD aerosol were observed for the remaining experiment time of about 2 h. The quantitative analysis of these experiments in terms of homogeneous nucleation rates of NAD will be published in a separate paper focusing on the distinction between volume- and surface-induced nucleation modes.[27] As for the present contribution, we will focus on two NAD aerosol spectra, Figure 3, which were obtained from different nucleation experiments: experiment B1 was conducted at an AIDA temperature of 193 K, experiment B2 at $T = 195$ K (shown in Figure 2). In experiment B1, the nitric acid/water ratio in the combined carrier gases which were added to the cooled AIDA chamber was slightly higher, leading to an initial composition of the nitric acid solution droplets of about 51 wt % HNO_3 compared to about 45 wt % HNO_3 in experiment B2. This, in addition to the lower temperature, leads to enhanced nucleation rates of NAD. Thus, α-NAD spectral signatures in the spectra series of experiment B1 already became visible at $t \sim 40$ min compared to $t \sim 190$ min in experiment B2.

Theory. Calculated NAD extinction spectra were fitted to the measured FTIR spectra, using α-NAD optical constants published by Toon et al.[5] and Niedziela et al.[7] as input data. In the first place, we assumed Mie theory to be valid to properly reproduce the observed extinction features of the NAD crystals. For the Mie fits, the algorithm provided by Bohren and Huffman[28] was extended to average the computed extinction cross sections over log-normally distributed particle sizes. The parameters of the aerosol size distribution (i.e., N = aerosol number density, σ_g = mode width, and CMD = count median diameter) were then used as fitting parameters, to retrieve the parameter set which minimized the summed squared residuals between experimental and calculated spectra. The downhill simplex method was employed as the optimization technique.[22,29]

In addition to Mie fits, T-matrix calculations were performed to study the effect of aspherical particle shapes on the NAD infrared extinction spectra. We used the extended precision FORTRAN T-matrix code for polydisperse, randomly oriented particles by Mishchenko and Travis,[30] restricted to rotationally symmetric aspherical particles. NAD crystals were modeled as prolate or oblate spheroids. Our fitting algorithm was modified to retrieve information about the size as well as shape distribution of the NAD crystals. For each wavenumber, a matrix of extinction cross sections σ was calculated by varying particle diameter D (defined as equal-volume sphere diameter) and aspect ratio Φ (i.e., the ratio of the horizontal to rotational axes).[30]

$$\begin{array}{ccccccc} & \Phi_1 & \Phi_2 & \cdots & \cdots & \Phi_M & \\ D_1 & \sigma_{11} & \sigma_{12} & \cdots & \cdots & \sigma_{1M} & \\ D_2 & \sigma_{21} & \ddots & & & \sigma_{2M} & \\ \vdots & \vdots & & \ddots & & \vdots & \\ \vdots & \vdots & & & \ddots & \vdots & \\ D_N & \sigma_{N1} & & & & \sigma_{NM} & \end{array} \quad (1)$$

For oblate spheroids, the particle diameter was incremented in 0.1 μm steps from 0.1 to 2.0 μm, whereas Φ was varied from 1 to 20 in steps of one. As the maximal convergent size parameters in T-matrix computations for prolate spheroids with an aspect ratio corresponding to the reciprocal oblate value are significantly reduced,[30] restrictions in D or Φ are imposed on the calculations of the σ matrix for prolate particle shapes. Here, we can vary D from 0.1 to 2.0 μm and Φ from 1:1, 1:2, 1:3, ..., to 1:10 or limit the particle sizes to a maximum of $D = 1.0$ μm to extend the computable aspect ratio up to 1:20. Using the σ matrix as input, we define for each particle size D_i a shape-averaged extinction cross section $\tilde{\sigma}$ with ϕ_k denoting the fraction of particles with aspect ratio Φ_k

$$\tilde{\sigma}(D_i,\tilde{\nu}_j) = \sum_{k=1}^{M} \phi_k \cdot \sigma(D_{ik},\tilde{\nu}_j) \quad (2)$$

with $\sum_{k=1}^{M} \phi_k = 1$. The size- and shape-averaged optical depth τ at a selected wavenumber may then be written as

$$\tau(\tilde{\nu}_j) = L \cdot \sum_{i=1}^{N} n(D_i) \cdot \tilde{\sigma}(D_i,\tilde{\nu}_j) \quad (3)$$

where L denotes the optical path length and $n(D_i)$ the number concentration of NAD particles in a particular size bin D_i. To

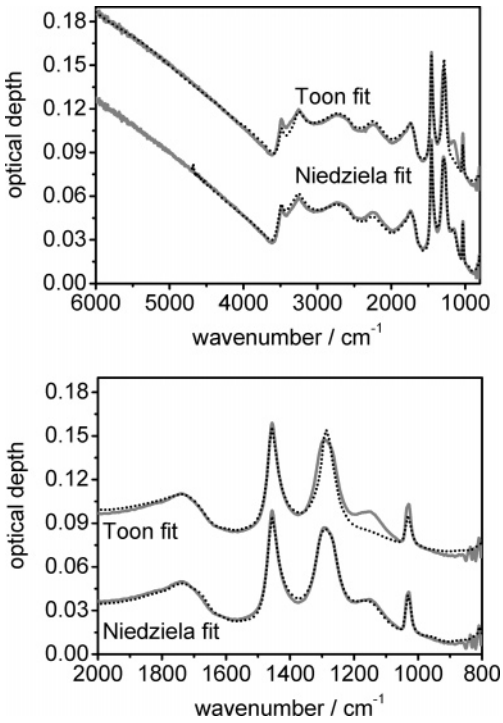

Figure 4. FTIR extinction spectrum of α-NAD generated in experiment A (gray solid lines) in comparison with best fit results from Mie calculations using the optical constants from Toon et al.[5] and Niedziela et al.[7] as input values (black dotted lines). The bottom panel shows an expanded view from 2000 to 800 cm^{-1}. For clarity, upper spectra on each panel are offset by 0.06 optical depth units.

reduce the number of fitting parameters in our algorithm, thereby increasing the uniqueness of our fit results, we constrained the size distribution $n(D_i)$ of the NAD crystals to log-normally distributed particle sizes. Further, we adopt a normal distribution of aspect ratios Φ_k to describe the shape distribution of NAD crystals and assume this shape distribution to be identical in all size bins D_i. Thus, the optimization procedure is limited to find the best parameter set of the size and shape distributions. Once again the downhill simplex method was used to minimize the residuals between measured and calculated extinction spectra.

Results and Discussion

Figure 3 shows a collection of the NAD infrared extinction spectra obtained in this work (i.e., from the experiments labeled A, B1, and B2). The spectra are offset for clarity, and the wavenumber range from 2000 to 800 cm^{-1} is expanded in the bottom part of the figure, revealing significant differences in band positions and intensities between the various FTIR spectra.

We start our discussion by analyzing the extinction spectrum obtained from experiment A. In Figure 4, this measured spectrum (solid line) is compared with the best fit results from Mie calculations (dotted line) using the α-NAD optical constants from Toon et al.[5] as well as Niedziela et al.[7] (refractive index data set for $T = 190$ K) as input values. In the latter case, the agreement between measured and calculated spectra is excellent. Note that the employed optical constants were derived from extinction spectra of NAD particles, which were generated by exactly the same method as in our experiment A, i.e., by shock freezing a water/nitric acid vapor mixture. Niedziela et al.[7] applied an iterative algorithm based on Mie theory to extract the optical constants from the recorded spectra. Hence, measured and calculated spectra are expected to compare well in this case.

More importantly, the thin-film α-NAD optical constants from Toon et al.,[5] whose derivation as a matter of course needs no explicit assumption on particle shape, also prove to accurately reproduce our measured spectrum in a Mie calculation. The only notable differences are a slight underestimation of the 1030 cm^{-1} peak optical depth and the reduced intensity of the 1160 cm^{-1} extinction band in the calculated spectrum, an aspect already addressed in previous studies.[7,31] Apparently, as indicated by Tisdale (cited in Disselkamp et al.[31]), the intensity of this band is somehow related to the film preparation method, since, for example, Koehler et al.[32] reported a thin-film α-NAD spectrum with a more pronounced 1160 cm $^{-1}$ feature (see Figure 4, spectrum c in their publication). As for the intensity of the 1030 cm^{-1} vibration, the resolution of only 8 wavenumbers in the Toon et al.[5] thin film infrared spectra might not be sufficient to fully resolve this sharp extinction band (fwhm < 20 cm^{-1}). Except for these slight spectral mismatches, however, Mie theory is obviously applicable to properly describe the infrared extinction features of NAD particles generated by shock freezing a H_2O/HNO_3 gas mixture, thus validating the approach of Niedziela et al.,[7] who used Mie theory to extract the optical constants from their measured NAD aerosol spectra. Two further studies are reported in the literature where NAD aerosol particles were formed by similar techniques. Bertram and Sloan[33] used a flow tube apparatus to study the freezing of NAD from liquid HNO_3/H_2O solution droplets on a time scale of 15 s. In the first sections of the flow tube, a liquid aerosol was formed at $T \sim 188$ K by homogeneous nucleation of an injected nitric acid/water vapor mixture. In the observation region of the flow cell, the temperature could be reduced to less than 160 K, causing the droplets to completely freeze to NAD. Barton et al.[34] directly injected a gas mixture of water and nitric acid in nitrogen into a static cluster cell, cooled to temperatures between 160 and 185 K, to study the formation conditions of nitric acid hydrates. Both groups recorded NAD infrared extinction spectra which closely resemble our spectrum of experiment A (see Figure 5, top spectrum[33] as well as Figure 1, spectrum b[34] in their respective publications).

Figure 3 shows that the NAD extinction spectra from our homogeneous nucleation experiments B1 and B2 reveal distinct deviations from the spectrum obtained in experiment A. First of all, the peak positions of the characteristic nitrate doublet feature with components at 1455 and 1290 cm^{-1} (experiment A) are shifted to about 1445 and 1270 (B1)/1265 (B2) cm^{-1}. Accompanying the band shift, the relative peak intensities in the nitrate doublet are inverted, the low-frequency component becoming more intense than the high-frequency one. This intensity change is even more pronounced in experiment B2 than in experiment B1, documenting that both the spectra B1 and B2, apart from showing systematic deviations from spectrum A, also differ slightly from each other. Interestingly, the 1160 cm^{-1} extinction band in spectrum A only appears as a shoulder in the spectra B1 and B2. Another striking difference is the intensity increase of the 1030 cm^{-1} band in relation to the nitrate doublet feature, accompanied by a slight red-shift of about 3−4 cm^{-1}. In the wavenumber regime from 6000 to 1500 cm^{-1} all spectra are quite similar, except for different scattering intensities above 4000 cm^{-1} due to different sizes of the generated NAD crystals.

Despite the spectral differences in the NO stretching region, spectra B1 and B2 still exhibit all spectral signatures characteristic of α-NAD as summarized by Grothe et al.,[17] i.e., the splitting of the OH stretching mode into two bands at 3490 and 3260 cm^{-1}, the asymmetric deformation mode of the oxonium ion at around 1730 cm^{-1}, and the sharp symmetric NO stretching mode at 1030 cm^{-1}, slightly shifted to about 1027 cm^{-1} in the

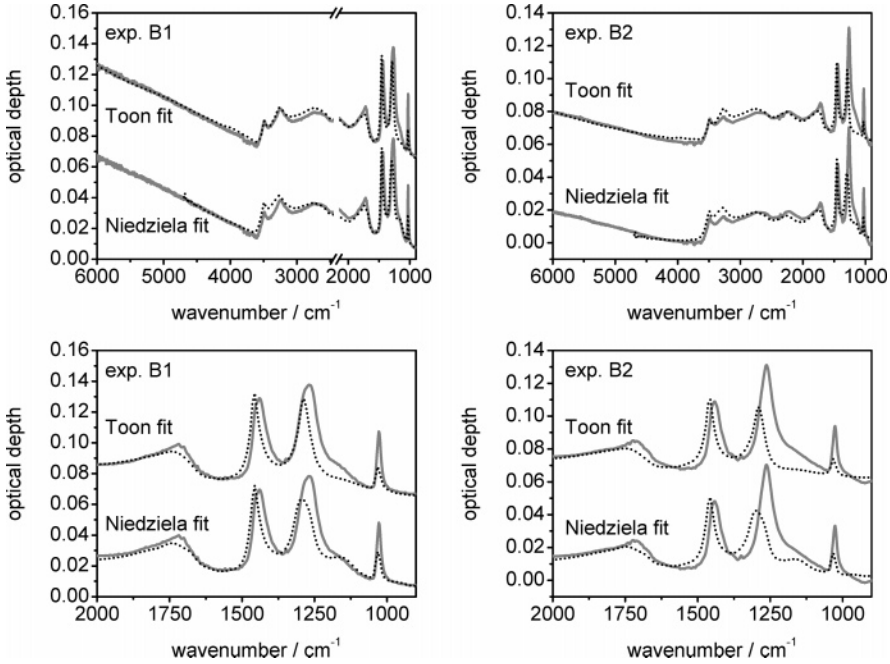

Figure 5. FTIR extinction spectra of α-NAD aerosols generated in experiments B1 (left) and B2 (right, gray solid lines) in comparison with best fit results from Mie calculations using optical constants from Toon et al.[5] and Niedziela et al.[7] as input values (black dotted lines). The lower panels show expanded views from 2000 to 800 cm^{-1}. For clarity, the top spectra are offset by 0.06 optical depth units in each panel.

spectra B1 and B2. None of the characteristics of β-NAD were observed, particularly the symmetric NO stretching mode which undergoes a significant shift to 1040 cm^{-1}. Also, the low-frequency shift of the nitrate doublet component from 1290 to 1265/1270 cm^{-1} is just opposite to the spectral change expected from the presence of β-NAD. We have not tried to induce a phase change by increasing the AIDA temperature, as our primary goal was to study nucleation of nitric acid hydrates over long time scales at uniform stratospheric temperatures. At these conditions, following the argumentation by Tizek et al.[16] in terms of Ostwald's step rule, the crystallization of the α-NAD modification should be favored since its structure more closely resembles the short-range order in the solution droplets. However, as is shown in Figure 5, Mie calculations using the α-NAD optical constants from Toon et al.[5] and Niedziela et al.[7] as input data poorly reproduce our spectra B1 and B2, with dramatic spectral mismatches in the NO stretching regime between 1500 and 1000 cm^{-1}.

Before offering an explanation for this spectral difference, we must exclude the possibility that we did not generate pure α-NAD particles in our nucleation experiments B1 and B2. Thus, we want to check whether the presence of other nitric acid hydrates such as NAM and NAT and/or unfrozen HNO_3/H_2O solution droplets could explain the deviations of our spectra B1 and B2 from the reference spectrum A. Figure 6 shows a collection of Mie theory-based infrared extinction spectra of NAM, α-NAT, β-NAT, α-NAD, and supercooled HNO_3/H_2O solution droplets (60 wt % HNO_3) for comparison with our measured spectrum B2 in the 2000−800 cm^{-1} region. This comparison reveals that spectrum B2 cannot be reproduced by co-adding suitable fractions of α- or β-NAT, NAM, or HNO_3/H_2O droplet spectra to the α-NAD spectrum. Hence, we conclude that indeed the pure α-NAD phase was formed in our slow nucleation experiments B1 and B2.

A possible effect of particle asphericity on the infrared spectrum of nitric acid dihydrate has only briefly been mentioned in some recent publications,[7,31] but no detailed simulations have been presented so far. In the following, we explore the

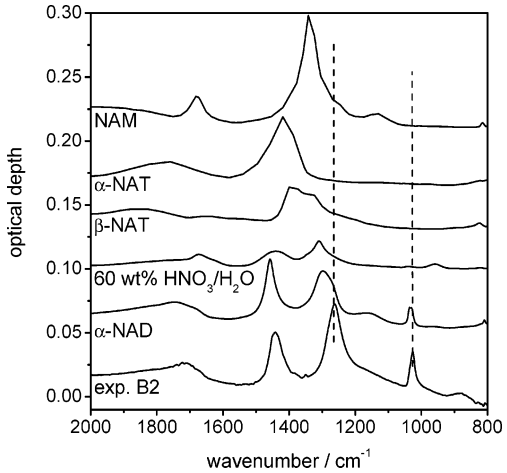

Figure 6. Comparison of the extinction spectrum of NAD aerosol generated in experiment B2 with Mie calculated infrared spectra of NAM, α-NAT, β-NAT, 60 wt % HNO_3/H_2O supercooled solution droplets, and α-NAD in the 2000−800 wavenumber regime. A median particle diameter of 0.5 μm was employed in the calculations. The individual spectra are offset for clarity. The optical constants from Toon et al.[5] for NAM, α-NAT, and β-NAT, from Norman et al.[26] for 60 wt % HNO_3/H_2O, and from Niedziela et al.[7] for α-NAD were used as input.

possibility that deviations from a spherical particle shape might explain the poor quality of the Mie fits to our spectra B1 and B2. To get an idea of the magnitude of this effect, Figures 7 and 8 show T-matrix calculated infrared extinction spectra of α-NAD for various spheroidal particle shapes. For fixed NAD particle diameters (i.e., equal-volume sphere diameters) of 1.0 μm (Figure 7) and 0.1 μm (Figure 8), the aspect ratios were continuously varied from unity (i.e., spherical particles) to 19:1 (oblate particles) as well as 1:19 (prolate particles). Our measured infrared spectra A and B2 are also shown for comparison.

It is striking that the asphericity-induced spectral changes lead to a much better match with our spectra B1 and B2, i.e., the

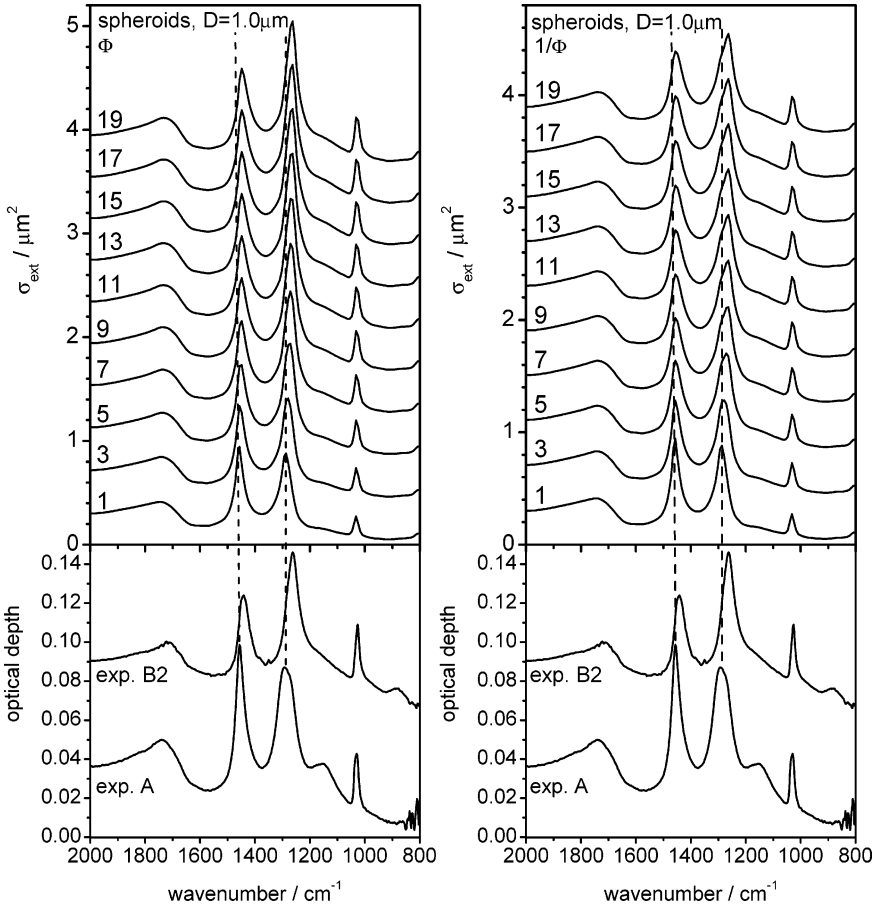

Figure 7. T-matrix calculations of the extinction cross sections (σ_{ext}) of NAD spheroids with an equal volume sphere diameter of 1.0 μm in the 2000 to 800 wavenumber regime in comparison with our measured infrared spectra from experiments A and B2. Left side: assuming oblate particles with aspect ratios from $\Phi = 1$ to $\Phi = 19$, right side: assuming prolate particles with aspect ratios from $1/\Phi = 1$ to $1/\Phi = 19$. Individual spectra are offset for clarity. The α-NAD optical constants from Toon et al.[5] were used as input.

red-shift and intensity change in the nitrate doublet feature as well as the increased intensity of the 1030 cm^{-1} extinction band are well reproduced. This is particularly true for oblate particle shapes, whereas the spectral changes are less pronounced in the calculations for prolate spheroids. A closer inspection of Figures 7 and 8 reveals that in the case of α-NAD the sensitivity of the infrared spectrum to the particle shape will by no means be removed when averaging over different NAD crystal sizes and shapes, as suggested by Niedziela et al.[7] Thus, we are strongly inclined to attribute the spectral differences between our spectra A and B1/B2 to the formation of strongly aspherical NAD crystals in our homogeneous nucleation experiments of type B. The subtle spectral differences between spectra B1 and B2 may be caused by different aspect ratios of the NAD crystals.

In Figures 9 and 10, our measured spectra are compared with best fit results using T-matrix calculations with the particle size and shape distributions as adjustable parameters, using the Toon et al.[5] α-NAD optical constants as input data. It is remarkable how well the spectra B1 and B2 are reproduced by the T-matrix fits for oblate particle shapes, as opposed to the poor quality of the corresponding Mie fits (see Figure 5). The only major discrepancies between measured and calculated spectra are different intensities in the ν_1 nitrate band at 1027 cm^{-1}, which may be attributed to the insufficient resolution of the Toon et al.[5] reference spectrum, as already discussed in the context of Figure 4. This extinction feature is better mimicked with the α-NAD optical constants from Niedziela et al.,[7] but at the same time, the intensity at 1160 cm^{-1} is significantly overestimated (see Figure 11 for an exemplary fit result with the Niedziela et al.[7] optical constants).

In general, the match between calculated and measured spectra is distinctly poorer for prolate than for oblate spheroids, especially in the 1500−1000 wavenumber regime, indicating that the shape of the generated NAD crystals is predominantly oblate. Concerning the retrieved size and shape distributions of the NAD crystals in the T-matrix fits, we are only able to specify a range of aspect ratios which best fits our measured spectra. Since a change in the aspect ratio Φ may be compensated to some extent by a different median particle diameter in the calculated spectra, similar fit results (i.e., nearly identical root-mean square deviations) can be obtained over a limited range of Φ values. For example, comparable fit results to spectrum B1 are obtained for near-monodispersed 1 μm NAD crystals with a median aspect ratio of 7 as well as for a broad NAD particle size distribution centered at 0.3 μm and a median aspect ratio of 6. When including these uncertainties resulting from the trade off between particle diameter and aspect ratio, the retrieved aspect ratios are in the range of $\Phi = 5-8$ for experiment B1 and $\Phi = 12-20$ for experiment B2. Since the spectral changes induced by an increasing aspect ratio are leveling off for $\Phi > 10$ (see Figure 7), the uncertainty range is somewhat larger in experiment B2.

As peak positions and relative peak intensities in the nitrate extinction regime between 1500 and 1000 cm^{-1} gradually change with increasing deviation from a spherical particle shape, FTIR extinction spectra prove to be sensitive indicators to the

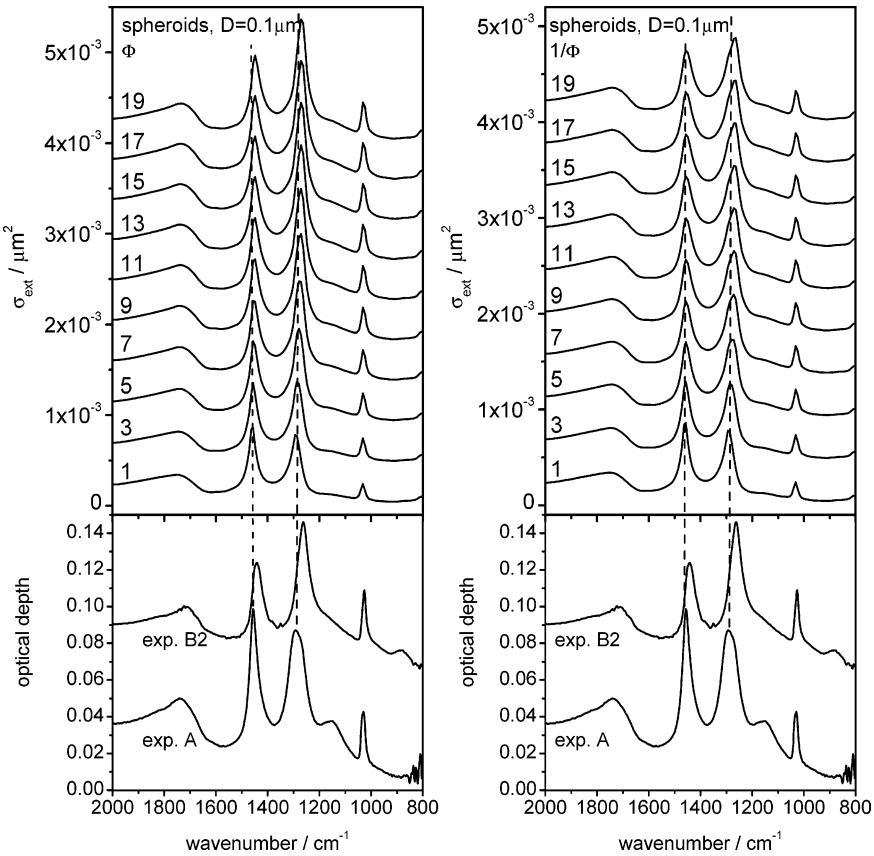

Figure 8. T-matrix calculations of the extinction cross sections (σ_{ext}) of NAD spheroids with an equal volume sphere diameter of 0.1 μm in the 2000 to 800 wavenumber regime in comparison with our measured infrared spectra from experiments A and B2. Left side: assuming oblate particles with aspect ratios from $\Phi = 1$ to $\Phi = 19$, right side: assuming prolate particles with aspect ratios from $1/\Phi = 1$ to $1/\Phi = 19$. Individual spectra are offset for clarity. The α-NAD optical constants from Toon et al.[5] were used as input.

degree of particle asphericity. It should, however, be noted that it is absolutely necessary to apply the fitting algorithm to the complete wavenumber range, i.e., not only to a microwindow covering the nitrate extinction regime. In the top part of Figure 12, we compare our measured spectrum B1 with the best fit result from a Mie calculation using the Niedziela et al.[7] optical constants of α-NAD as input data, limited to the 2000−800 cm^{-1} spectral range.

The fairly good agreement between measured and calculated spectra (retrieved median particle diameter ~ 2 μm) seems to be in striking contradiction with our previous argument, i.e., that Mie theory is not adequate to accurately reproduce this extinction spectrum. However, it is just a result of the limited wavenumber range used in the fit that the presence of aspherical particles might be overlooked. The lower part of Figure 12 shows what the Mie calculated spectrum looks like at wavenumbers >2000 cm^{-1}, documenting that measured and calculated spectra largely deviate in this regime. Thus, the increased scattering contribution of large NAD spheres with $D \sim 2$ μm in comparison to 1-μm-sized spheres (see Figure 7, spectrum for $\Phi = 1$) may provoke to some extent the same spectral changes in the 2000−800 cm^{-1} region of the NAD extinction spectrum as does an increasing aspect ratio (Figure 7). Light scattering by 2 μm NAD spheres at wavenumbers greater than 2000 cm^{-1}, however, is too pronounced to accurately mimick the measured extinction spectrum. Hence, constraining the fitting regime may lead to incorrect retrievals of PSC microphysical parameters.

Our retrieved aspect ratios are significantly larger than those commonly used in model calculations analyzing lidar observations of polar stratospheric clouds. Liu and Mishchenko[12] performed extensive T-matrix calculations for oblate and prolate cylinders as well as spheroids, thereby establishing likely ranges of PSC particle microphysical parameters (i.e., shapes and effective radii) which best reproduced measured lidar data (backscatter ratio, backscattering depolarization ratio, as well as backscatter and depolarization color indices). In a similar study, Brooks et al.[11] employed measured PSC size distributions as input for T-matrix calculations of aerosol backscatter ratios and aerosol depolarization ratios, which were then compared to observed lidar measurements. In both studies, no aspect ratios exceeding two (or lower than 0.5 in the case of prolate shapes) were examined, certainly also a consequence of the larger size parameters at visible wavelengths which limit the range of computable aspect ratios with the T-matrix code.[30] However, the calculations clearly demonstrate that for example the correlation between depolarization ratio and particle asphericity is complex. Zakharova and Mishchenko,[35] for example, have shown that highly aspherical ice spheroids with aspect ratios of 20:1 or 1:20 reveal significantly weaker backscattering depolarizations than crystals with $\Phi = 2$ or 0.5. Thus, it is recommended to check whether more extreme aspect ratios would also be consistent with the lidar data. As our simulation experiments of type B mimic one potential pathway for the formation of crystalline PSCs, i.e., the nucleation of NAD or NAT out of supercooled ternary $HNO_3/H_2O/H_2SO_4$ solution droplets, one should not exclude the possibility that highly aspherical, maybe platelike nitric acid hydrates are formed in the polar stratosphere, as inferred from our measured infrared spectra.

We conclude our discussion by comparing our results with a study by Disselkamp et al.,[31] who analyzed the crystallization

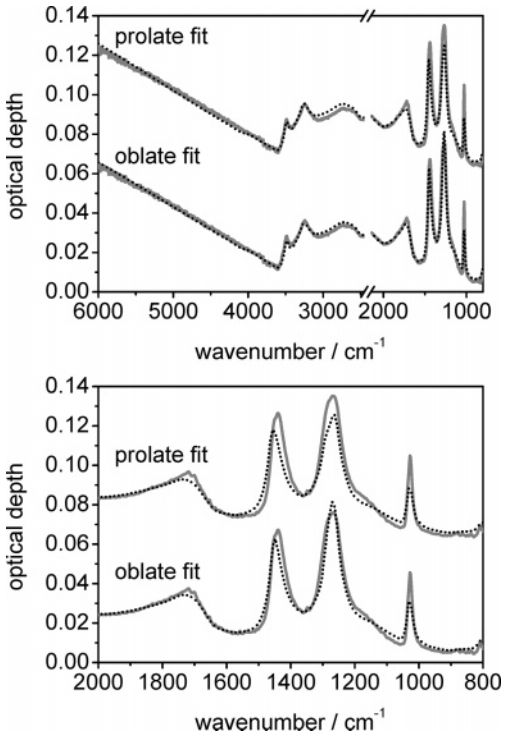

Figure 9. Experimental FTIR extinction spectrum of α-NAD generated in experiment B1 (gray solid lines) in comparison with best fit results based on T-matrix calculations for oblate and prolate spheroids using the optical constants from Toon et al.[5] (black dotted lines). The bottom panel shows an expanded view from 2000 to 800 cm^{-1}. For clarity, the top spectra are offset by 0.06 optical depth units in each panel.

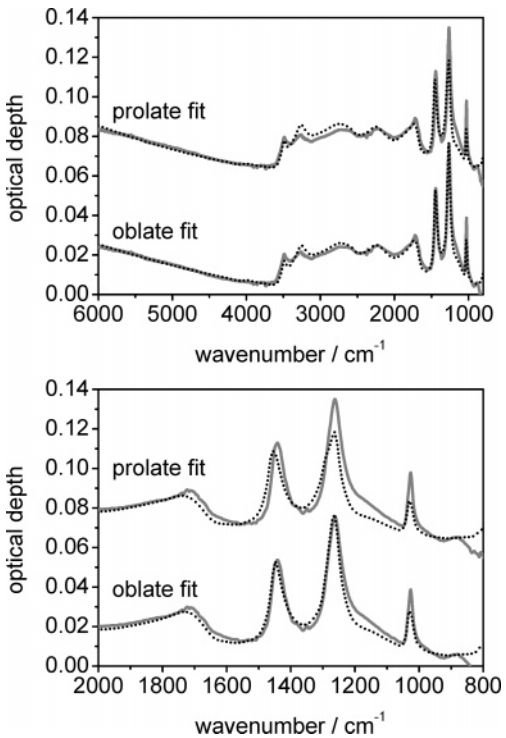

Figure 10. FTIR extinction spectrum of α-NAD aerosol generated in experiment B2 (gray solid lines) in comparison with best fit results from T-matrix calculations for oblate and prolate spheroids using the optical constants from Toon et al.[5] (black dotted lines). The bottom panel shows an expanded view from 2000 to 800 cm^{-1}. For clarity, the top spectra are offset by 0.06 optical depth units in each panel.

kinetics of nitric acid dihydrate aerosols using FTIR extinction spectroscopy. The authors recorded an infrared spectrum of

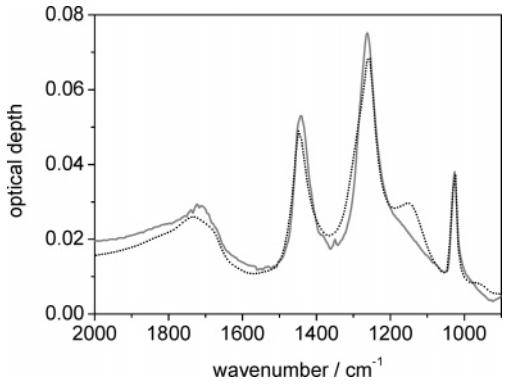

Figure 11. FTIR extinction spectrum of α-NAD aerosol generated in experiment B2 (gray solid line) in comparison with the best fit result based on T-matrix calculations for oblate spheroids using the optical constants from Niedziela et al.[7] (black dotted line).

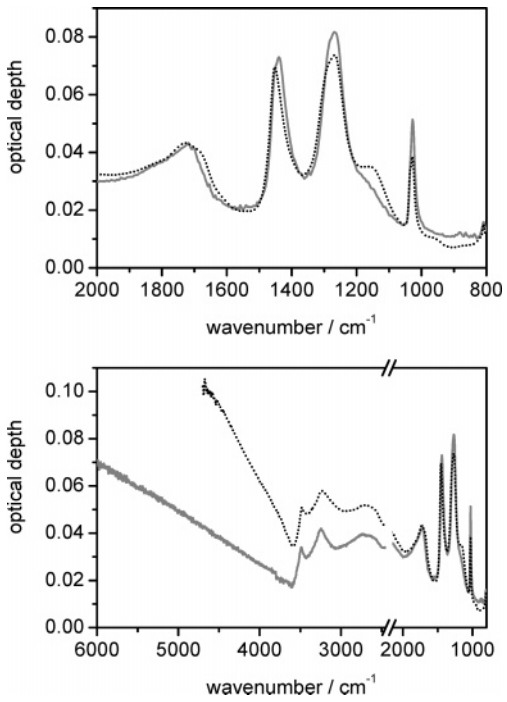

Figure 12. Upper panel: FTIR extinction spectrum of α-NAD aerosol generated in experiment B1 (gray solid line) in comparison with the best fit result from a Mie calculation using the optical constants from Niedziela et al.[7] (black dotted line), when limiting the fitting interval to the 2000−800 cm^{-1} range. In the bottom panel, the size distribution parameters retrieved from the Mie fit ($\sigma_g \sim 1.001$, CMD ~ 2.0 μm) were used to calculate the α-NAD extinction spectrum in the complete range from 4700 to 800 cm^{-1} (black dotted line). Spectrum B1 is shown for comparison (gray solid line).

α-NAD which to some extent resembles the spectra obtained in our nucleation experiments of type B. Figure 7 in their publication shows a series of infrared spectra documenting the growth of NAD crystals from 2:1 H_2O/HNO_3 solution droplets at $T = 202$ K over a time scale of 95 s. The resulting extinction spectrum of the NAD crystals (their spectrum d) clearly shows the spectral characteristics of aspherical particles, i.e., an increased intensity at 1030 cm^{-1} and inverted peak intensities of the nitrate doublet feature, though not as pronounced as in our spectra B1 and B2. The authors applied Mie theory to fit their NAD spectrum, thereby retrieving a nearly monodispersed size distribution with $D = 1.08$ μm. Unfortunately, the Mie simulation is not shown, but we know from our own T-matrix calculations (Figure 7 in this paper) how an α-NAD extinction spectrum for "spherical" particles of 1 μm diameter should look

like in the 2000 to 800 wavenumber region: it is just the spectrum calculated for $\Phi = 1$. Clearly, the NAD spectrum of Disselkamp et al.[31] is only poorly reproduced by the Mie calculation in this spectral range, and a much better fit would have been obtained with the spheroidal model for an aspect ratio of about 3, just by visual inspection of our T-matrix calculations shown in Figure 7. Using the same aerosol settling chamber as in the Disselkamp et al.[31] study, Prenni et al.[36] performed additional freezing experiments for more dilute nitric acid solution droplets. For instance, they used a 2.5:1 H_2O/HNO_3 aerosol, which closely corresponds to the composition of our nitric acid solution droplets in experiments B1 and B2 just by the time when the signatures of α-NAD were first observed in our infrared spectra (Figure 2). Unfortunately, freezing of the H_2O/HNO_3 droplets to α-NAD was not completed at the end of their maximum observation time (see Figure 8 in their publication);[36] hence, no infrared spectrum of pure α-NAD was obtained which could be compared to our spectra B1 and B2.

Obviously, the degree of the asphericity of NAD crystals originating from supercooled solution droplets can be quite variable. Rapid freezing of supercooled HNO_3/H_2O solution droplets, induced by reducing the temperature in a flow tube apparatus, leads to an α-NAD extinction spectrum which can be accurately reproduced using Mie theory.[33] Slight deviations from spherical are observed in the aerosol chamber study by Disselkamp et al.,[31] where nucleated NAD crystals are allowed to grow by mass transfer from unfrozen solution droplets over a short time period of 1.5 min. In our nucleation studies, this time frame of crystal growth in a supersaturated environment is significantly longer (though still significantly shorter than polar stratospheric time scales). Apparently, the nucleated NAD crystals thereby gradually adopt the high degree of particle asphericity, as observed in experiments B1 and B2.

Conclusions

Infrared extinction spectra of α-NAD crystals homogeneously nucleated from supercooled HNO_3/H_2O solution droplets at $T = 193$ and 195 K reveal significant spectral differences from infrared spectra of α-NAD particles generated by rapid cooling of a HNO_3/H_2O gas mixture. Whereas in the latter case Mie theory is applicable to properly describe the α-NAD extinction features, spectral changes indicate the formation of highly aspherical NAD crystals in the homogeneous nucleation studies. T-matrix calculations using a spheroidal particle model showed that oblate particle shapes best fitted our recorded infrared spectra. Since exactly these nucleation experiments of type B represent a potential pathway for the formation of solid nitric acid hydrates in the winter polar stratosphere, care has to be taken in analyzing lidar or infrared spectral data of PSC type Ia particles when making assumptions about the particle shape. Thus, current inversion methods for the characterization of aerosol particles from, for example, infrared transmission spectra of the ATMOS (Atmospheric Trace Molecule Spectroscopy) instrument[37] or mid-IR limb emission spectra from MIPAS (Michelson Interferometer for Passive Atmospheric Sounding)[10] should be checked to quantify the effect of particle asphericity on the retrieval results. As a further complication, the degree of particle asphericity may be variable, since significantly different aspect ratios were retrieved for NAD particles which had nucleated at slightly different chamber temperatures. As already indicated in the Experimental Section, both the lower temperature and the higher initial nitric acid content of the HNO_3/H_2O solution droplets in experiment B1 gave rise to enhanced NAD nucleation rates, thereby shortening the overall time period of NAD nucleation and crystal growth under supersaturated conditions compared to experiment B2. This obviously leads to a lower degree of particle asphericity of the nucleated NAD crystals. As will be further explored in a manuscript in preparation, we never observed any spectral indication of NAT formation in our nucleation experiments, covering NAT saturation ratios (S_{NAT}) of about 16−26 (increasing with increasing nitric acid content in the solution droplets) and time scales of up to 4 h.[27]

In addition to the spheroidal model used to analyze our NAD extinction spectra, further techniques have become available to calculate the optical properties of arbitrarily shaped particles, containing no symmetry axes. Reichardt et al.,[13] for example, employed the finite-difference time-domain (FDTD) method to calculate PSC optical properties for hexagonal and asymmetric polyhedral crystals, emphasizing that there is so far no convincing direct observational evidence of predominant PSC particle shapes which would validate the use of the spheroidal model for retrieving PSC microphysical parameters. In this context, further experiments in the AIDA chamber are considered with the objective to grow NAD crystals to sizes which can be detected with an optical particle imager. Such an instrument which will exceed the resolving power of a commercially available CPI (cloud particle imaging) system[38] is presently under construction.[39] Direct evidence of the NAD crystal shape which could be compared with aspect ratios deduced by techniques such as FTIR extinction spectroscopy, aerosol scattering, and depolarization measurements is needed to test the accuracy by which PSC microphysical parameters can be retrieved from remote sensing data.

Acknowledgment. The authors are grateful for the continuous support by all members of the AIDA staff. We thank H. Bunz for computational assistance in the T-matrix calculations and M. Höpfner for helpful discussions about satellite observations of PSCs. The work has been funded by BMBF (AFO2000 Project POSTA, 07ATF04).

References and Notes

(1) Zasetsky, A. Y.; Sloan, J. J.; Escribano, R.; Fernandez, D. *Geophys. Res. Lett.* **2002**, *29*, 2071.

(2) Toon, O. B.; Tabazadeh, A.; Browell, E. V.; Jordan, J. *J. Geophys. Res. (Atmos.)* **2000**, *105*, 20589.

(3) Schreiner, J.; Voigt, C.; Weisser, C.; Kohlmann, A.; Mauersberger, K.; Deshler, T.; Kröger, C.; Rosen, J.; Kjome, N.; Larsen, N.; Adriani, A.; Cairo, F.; Di Donfrancesco, G.; Ovarlez, J.; Ovarlez, H.; Dörnbrack, A. *J. Geophys. Res.* **2003**, *108* (D5), 8313.

(4) Voigt, C.; Larsen, N.; Deshler, T.; Kröger, C.; Schreiner, J.; Mauersberger, K.; Luo, B. P.; Adriani, A.; Cairo, F.; Di Donfrancesco, G.; Ovarlez, J.; Ovarlez, H.; Dörnbrack, A.; Knudsen, B.; Rosen, J. *J. Geophys. Res.* **2003**, *108* (D5), 8331.

(5) Toon, O. B.; Tolbert, M. A.; Koehler, B. G.; Middlebrook, A. M.; Jordan, J. *J. Geophys. Res. (Atmos.)* **1994**, *99*, 25631.

(6) Biermann, U. M.; Luo, B. P.; Peter, T. *J. Phys. Chem. A* **2000**, *104*, 783.

(7) Niedziela, R. F.; Miller, R. E.; Worsnop, D. R. *J. Phys. Chem. A* **1998**, *102*, 6477.

(8) Norman, M. L.; Miller, R. E.; Worsnop, D. R. *J. Phys. Chem. A* **2002**, *106*, 6075.

(9) Richwine, L. J.; Clapp, M. L.; Miller, R. E.; Worsnop, D. R. *Geophys. Res. Lett.* **1995**, *22*, 2625.

(10) Höpfner, M. *J. Quant. Spectrosc. Radiat. Transfer* **2004**, *83*, 93.

(11) Brooks, S. D.; Toon, O. B.; Tolbert, M. A.; Baumgardner, D.; Gandrud, B. W.; Browell, E. V.; Flentje, H.; Wilson, J. C. *J. Geophys. Res.* **2004**, *109*, D02212.

(12) Liu, L.; Mishchenko, M. I. *J. Quant. Spectrosc. Radiat. Transfer* **2001**, *70*, 817.

(13) Reichardt, J.; Reichardt, S.; Yang, P.; McGee, T. J. *J. Geophys. Res.* **2002**, *107* (D20), 8282.

(14) Lebrun, N.; Mahe, F.; Lamiot, J.; Foulon, M.; Petit, J. C. *Acta Crystallogr. C* **2001**, *57*, 1129.

(15) Lebrun, N.; Mahe, F.; Lamiot, J.; Foulon, M.; Petit, J. C.; Prevost, D. *Acta Crystallogr. B* **2001**, *57*, 27.
(16) Tizek, H.; Knözinger, E.; Grothe, H. *Phys. Chem. Chem. Phys.* **2002**, *4*, 5128.
(17) Grothe, H.; Myhre, C. E. L.; Tizek, H. *Vib. Spectrosc.* **2004**, *34*, 55.
(18) Tisdale, R. T.; Prenni, A. J.; Iraci, L. T.; Tolbert, M. A.; Toon, O. B. *Geophys. Res. Lett.* **1999**, *26*, 707.
(19) Escribano, R.; Couceiro, M.; Gomez, P. C.; Carrasco, E.; Moreno, M. A.; Herrero, V. J. *J. Phys. Chem. A* **2003**, *107*, 651.
(20) Fernandez, D.; Botella, V.; Herrero, V. J.; Escribano, R. *J. Phys. Chem. B* **2003**, *107*, 10608.
(21) Möhler, O.; Stetzer, O.; Schaefers, S.; Linke, C.; Schnaiter, M.; Tiede, R.; Saathoff, H.; Krämer, M.; Mangold, A.; Budz, P.; Zink, P.; Schreiner, J.; Mauersberger, K.; Haag, W.; Kärcher, B.; Schurath, U. *Atmos. Chem. Phys.* **2003**, *3*, 211.
(22) Wagner, R.; Mangold, A.; Möhler, O.; Saathoff, H.; Schnaiter, M.; Schurath, U. *Atmos. Chem. Phys.* **2003**, *3*, 1147.
(23) Wagner, R.; Naumann, K.-H.; Mangold, A.; Möhler, O.; Saathoff, H.; Schurath, U. Aerosol chamber study of PSC type Ib particles: Optical constants and N_2O_5 uptake on supercooled $H_2SO_4/H_2O/HNO_3$ solution droplets at stratospheric temperatures, manuscript in preparation, 2005.
(24) Knopf, D. A.; Zink, P.; Schreiner, J.; Mauersberger, K. *Aerosol. Sci. Technol.* **2001**, *35*, 924.
(25) Möhler, O.; Büttner, S.; Linke, C.; Schnaiter, M.; Saathoff, H.; Stetzer, O.; Wagner, R.; Krämer, M.; Mangold, A.; Ebert, V.; Schurath, U. Effect of Sulphuric Acid Coating on Heterogeneous Ice Nucleation by Soot Aerosol Particles. *J. Geophys. Res.* **2004**, submitted.
(26) Norman, M. L.; Qian, J.; Miller, R. E.; Worsnop, D. R. *J. Geophys. Res. (Atmos.)* **1999**, *104*, 30571.
(27) Stetzer, O.; Bunz, H.; Möhler, O.; Saathoff, H.; Schnaiter, M.; Schurath, U.; Wagner, R. Volume versus surface nucleation of NAD under simulated PSC conditions. Manuscript in preparation, 2005.
(28) Bohren, C. F.; Huffman, D. R. *Absorption and Scattering of Light by Small Particles*; John Wiley & Sons: New York, 1983.
(29) Press, W. H.; Teukolsky, S. A.; Vetterling, W. T.; Flannery, B. P. *Numerical Recipes in C: The Art of Scientific Computing*; Cambridge University Press: Cambridge, 1992.
(30) Mishchenko, M. I.; Travis, L. D. *J. Quant. Spectrosc. Radiat. Transfer* **1998**, *60*, 309.
(31) Disselkamp, R. S.; Anthony, S. E.; Prenni, A. J.; Onasch, T. B.; Tolbert, M. A. *J. Phys. Chem.* **1996**, *100*, 9127.
(32) Koehler, B. G.; Middlebrook, A. M.; Tolbert, M. A. *J. Geophys. Res. (Atmos.)* **1992**, *97*, 8065.
(33) Bertram, A. K.; Sloan, J. J. *J. Geophys. Res. (Atmos.)* **1998**, *103*, 3553.
(34) Barton, N.; Rowland, B.; Devlin, J. P. *J. Phys. Chem.* **1993**, *97*, 5848.
(35) Zakharova, N. T.; Mishchenko, M. I. *Appl. Opt.* **2000**, *39*, 5052.
(36) Prenni, A. J.; Onasch, T. B.; Tisdale, R. T.; Siefert, R. L.; Tolbert, M. A. *J. Geophys. Res. (Atmos.)* **1998**, *103*, 28439.
(37) Zasetsky, A. Y.; Khalizov, A. F.; Sloan, J. J. *Appl. Opt.* **2004**, *43*, 5503.
(38) Heymsfield, A. J.; Bansemer, A.; Field, P. R.; Durden, S. L.; Stith, J. L.; Dye, J. E.; Hall, W.; Grainger, C. A. *J. Atmos. Sci.* **2002**, *59*, 3457.
(39) Schnaiter, M. *Personal communication*.